TECHNICAL PAPER

JOURNAL OF THE SOUTH AFRICAN INSTITUTION OF CIVIL ENGINEERING
ISSN 1021-2019 (print) | ISSN 2309-8775 (online)
Vol 66 No 4, December 2024, Pages 2–15, Paper 1680

Investigations of the impact of considering different numerical modelling techniques for determining seismic damage at the dam-foundation interface of the stepped abutment of a concrete gravity dam: A case study on the Beni-Haroun Dam

Z Abdelli, A Becheur



ZAHIA ABDELLI, who specialises in hydraulic structures, is a PhD student at the University of Béjaïa, Algeria. Her research focuses on fluid and structural mechanics, numerical modelling, fluid-structure interaction, and the analysis and design of concrete dams.

Contact details:
ZAHIA ABDELLI
University of Bejaia,
Faculty of Technology
Laboratory of Applied Hydraulic and Environment (LRHAE)
06000, Bejaia, Algeria
E: zahia.abdelli@univ-bejaia.dz



DR ABDELHAMID BECHEUR, who has more than 28 years of experience in the numerical analysis of structures, is a senior lecturer in Civil and Mechanical Engineering at the University of Béjaïa, Algeria. His research interests include advanced nonlinear calculations, such as nonlocal damage mechanics (explored in his Master's research) and error estimation in contact mechanics (which was the focus of his PhD research, completed in 2008 in collaboration with the University of Picardie Jules Verne in France). He has extensive experience teaching Master's students in finite element methods and metallic structure analysis.

Contact details:
ABDELHAMID BECHEUR
University of Bejaia
Faculty of Technology
Laboratory of Applied Hydraulic and Environment (LRHAE)
06000, Bejaia, Algeria
E: abdelhamid.becheur@univ-bejaia.dz

This paper investigates how accounting for contact conditions and a step abutment in the foundation affects the seismic damage behaviour of concrete gravity dams. For this purpose, a pushover analysis was conducted utilising two distinct calculation models based on continuum damage mechanics. The first model uses a continuous mesh between the dam and the soil foundation without modelling any discrete interfaces, while the second considers the dam and soil meshes separately with contact relations. To improve accuracy, the numerical simulations were conducted for each case with three different damage models. The results indicate how considering contact conditions has a significant impact not only on the overall seismic response but also on the distribution and progression of the damage field in the dam. More precisely, the areas where damage occurs in the vicinity of the foundation zones differ between these two models. The first model results indicate damage first appearing near the heel, while with the second model the damage begins near the abutment. This is demonstrated using the Beni-Haroun gravity dam as a structural case study.

Keywords: contact problem, calculation model, damage model, step abutment, pushover analysis

INTRODUCTION

The contact conditions between a concrete gravity dam and its foundation are of great importance for maintaining its structural integrity and stability. The interface plays a critical role in the equilibrium and the transmission of various loads and stresses. Consequently, predicting the damaged and contact zones within the dam and their evolution during seismic excitation is a challenging task that is often accomplished using finite element methods. However, many studies neglect these contact relations and use continuous meshes instead. Conversely, numerous other works consider these conditions and the resulting friction phenomenon in their formulations. This article aims to investigate the impact of accounting for these contact conditions with the presence of a step abutment in the foundation on the seismic damage behaviour of concrete gravity dams.

In the framework of damage mechanics theory, a local representative internal damage model is currently used in order to simulate the distribution and evolution of damage

Abdelli Z, Becheur A. Investigations of the impact of considering different numerical modelling techniques for determining seismic damage at the dam-foundation interface of the stepped abutment of a concrete gravity dam: A case study on the Beni-Haroun Dam. J. S. Afr. Inst. Civ. Eng. 2024:66(4), Art. #1680, 14 pages. http://dx.doi.org/10.17159/2309-8775/2024/v66n4a1

The *Journal of the South African Institution of Civil Engineering*, which is distributed internationally, is a peer-reviewed, open-access journal licensed under a Creative Commons Attribution Licence (CC BY-NC-ND). Readers may therefore freely use and share the content as long as they credit the original creator and publisher, do not change the material in any way, and do not use it commercially. Copyright of this article remains with the authors.

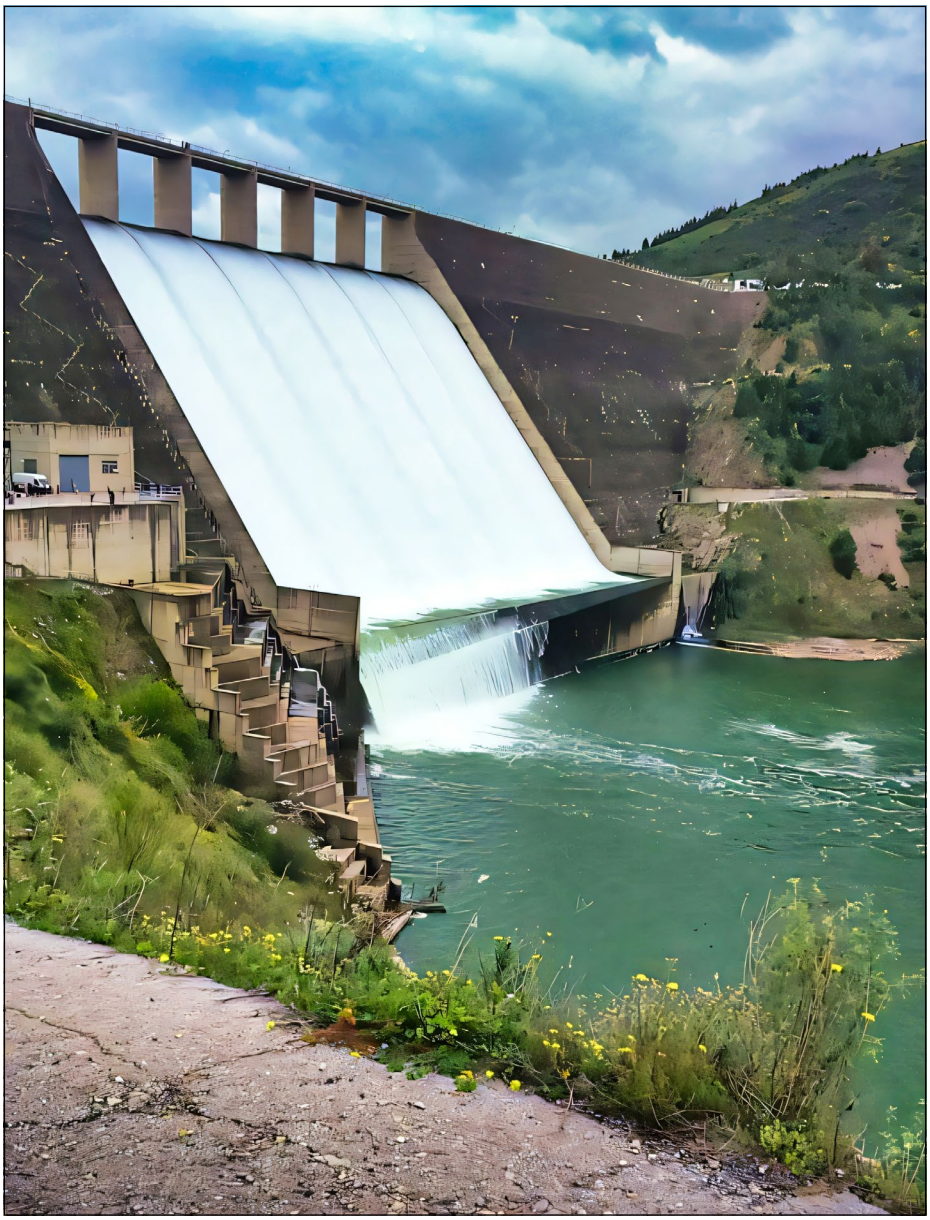

Figure 1 View of Beni-Haroun concrete gravity dam

fields, resulting from the propagation and coalescence of micro-cracks and micro-voids in a structure. This variable characterises the density and orientation of these micro-defects. Kachanov (1958) first introduced the formulation, which was subsequently improved by Rabotnov (1959). Since then, numerous isotropic and anisotropic models have been developed. Among these are the Mazars model (Mazars 1986), the Modified Von Mises model (De Vree *et al* 1995) and the RICRAG model (Richard *et al* 2010). However, according to Bažant (1986), local models are not suitable for materials with a softening behaviour. Indeed, when the mesh is refined, damage localisation tends to occur in smaller areas, leading to a dissipation of energy during rupture that eventually vanishes, which is physically unacceptable (Needleman 1988). To address this mesh dependence, several localisation limiters have been developed. Pijaudier-Cabot and Bažant (1987) developed a method that was widely used for a long time. Giry *et al* (2011) proposed an improved version of this non-local regularisation technique, known as the stress-based method. The three aforementioned damage models and the previous regularisation technique will be briefly presented in the following section of this paper, and will be used in our simulations performed by using Cast3M (2023) calculation code developed by the CEA in France.

Furthermore, in order to achieve our objective, a pushover analysis will be conducted employing two distinct calculation models. The first model involves using a continuous mesh between the dam and the foundation without interfaces, while the second model considers the dam and foundation meshes separately with contact relations. For this purpose, the typical structure of the Beni-Haroun gravity dam will be analysed. This dam, situated in a seismic zone in northern Algeria, is considered one of the most significant hydraulic constructions in Africa (see Figure 1). [For more information about this structure, a study conducted by Si-Chaib *et al* (2018) can serve as a reference.]

In this paper the authors reassessed the dam's dynamic behaviour using a progressive approach as part of a new seismic safety assessment. In addition, and as illustrated in Figure 2, our choice of this dam is also due to its principal characteristic, namely the presence of an abutment step in the foundation, which acts as a partial obstacle against sliding. Moreover, to account for the physical phenomenon of friction, which plays a critical role in ensuring the dam's stability, the analysis employs Coulomb's law of friction, a widely used approach considered in literature to be among the most realistic. Additionally, the computations will account for uplift pressures and hydrodynamic fluid effects by using Westergaard's added masses method (Westergaard 1933).

For the case of damage simulations without modelled interfaces, it is common practice to use a continuous mesh between the foundation and the dam. However, this approach has limitations since the computed stresses are highly sensitive to mesh density at singularity (re-entrant corner) points. These points are located at the heel and toe of the dam where stress peaks occur, as shown in Figure 2. In order to obtain more realistic field stresses Durieux and Van Rensburg (2016) used the plastic Drucker-Prager yield model in their works. However, despite the existence of these zones of singularities, several authors continue to employ this contactless method. Indeed, Calayir and Karaton (2005) introduced a damage model that includes a second-order tensor as an internal variable and incorporates strain-softening behaviour. Faggiani *et al* (2021) and Enzell *et al* (2021) employed the Concrete Damage Plasticity (CDP) model proposed by Lee and Fenves (1998). Vorlet *et al* (2021) utilised a coupled damage plasticity model for concrete based on the microplane formulation developed by Zreid and Kaliske (2018). It is also worth mentioning the works of Bhattacharjee and Léger (1994) who initially developed the continuous crack approach. Subsequently, Léger and Leclerc (1996) made improvements. This approach, also known as the smeared crack approach, is characterised by its primary feature of not capturing individual cracks. Additionally, the works of Cai *et al* (2008) can be cited for their development of a smeared crack model that incorporates either linear or bilinear softening.

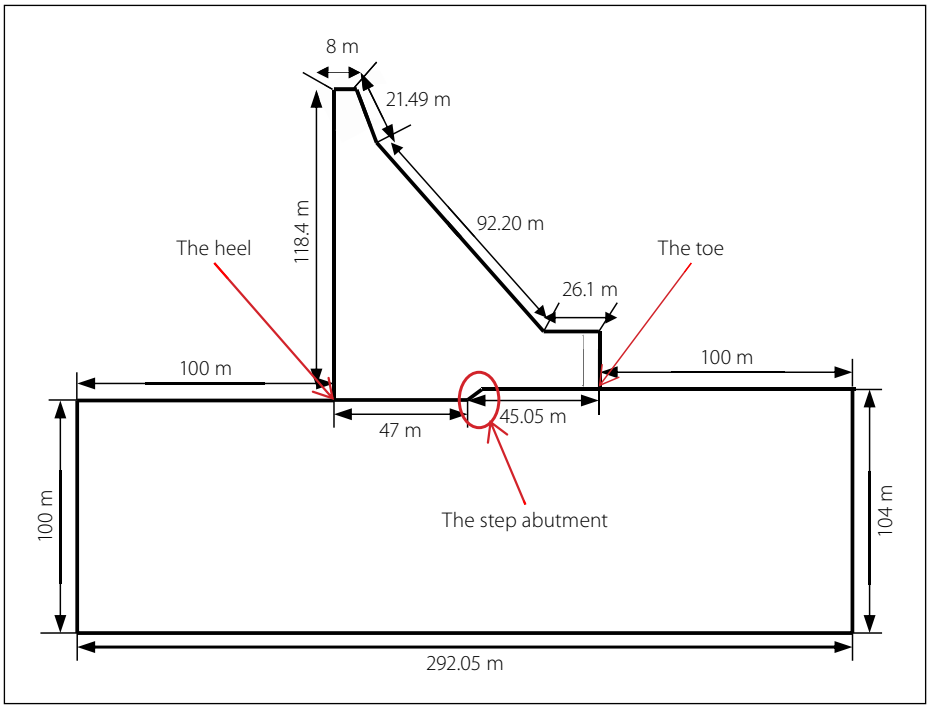

Figure 2 Dimensions of Beni-Haroun concrete gravity dam

Although the difficulties arising from these singularity points can be reduced by using the contact approach, which produces steep strain gradient areas instead, the literature on simulating contact between dams and their foundations using continuous damage models appears to be limited. However, for the case of a small dam with abutment in its foundation, Jabbar *et al* (2021) investigated the potential enhancement of seismic resistance in gravity dams through the utilisation of stepped bases.

NON-LOCAL DAMAGE MODELS

Formulated within the framework of thermodynamics for irreversible processes, damage models have been developed to predict the failure of concrete and quasi-brittle materials. For the case of isotropic damage, which is the focus of this study, each point within a structure is associated with an internal damage variable, represented by a scalar parameter d, defined within the interval [0, 1] such as the loss of stiffness associated with the mechanical degradation of the material, as follows:

$$\sigma = (1 - d)\mathbf{H}\varepsilon \quad (1)$$

Where: σ, ε and $\mathbf{H}$ denote the Cauchy stress, small strain and elastic Hook tensors respectively. Specifically, $d = 0$ indicates an undamaged point, while $d = 1$ signifies a completely damaged point. Another assumption is that d depends on a state variable Y, which represents the local damage energy released rate, which in turn is a function of the strains:

$$Y = Y(\varepsilon) \quad (2)$$

However, to address the aforementioned localisation issues, it becomes necessary to employ a combined regularisation method, often referred to as a "localisation limiter".

Indeed, the fundamental concept behind non-local damage models involves the averaging of this state variable Y in the vicinity of each point. In other words, it consists in averaging the damage threshold surface in the vicinity of the considered point. This allows the establishment of the definition of a non-local state variable, denoted Y^{nl}, by using either the classic method of Pijaudier-Cabot and Bažant (1987) or the most recent stress-based method of Giry *et al* (2011) which was adopted for the present calculations. For this purpose, the local damage energy released rate Y is replaced by the non-local one Y^{nl} such as:

$$Y^{nl}(\boldsymbol{x}) = \frac{\int_{\Omega(\boldsymbol{x})} W(\boldsymbol{x} - \boldsymbol{s})\, Y(\boldsymbol{s})\, ds}{\int_{\Omega(\boldsymbol{x})} W(\boldsymbol{x} - \boldsymbol{s})\, ds} \quad (3)$$

$W(\boldsymbol{x} - \boldsymbol{s})$ is the weight or also called Gauss distribution function defining the interaction between the considered point located with $\boldsymbol{x}$ and the neighbouring points located with s inside the volume of the structure $\Omega(\boldsymbol{x})$ such as:

$$W(\boldsymbol{x} - \boldsymbol{s}) = exp\left[-\left(\frac{2||\boldsymbol{x} - \boldsymbol{s}||}{l_c \cdot \rho(\boldsymbol{x}, \sigma_{prin}(\boldsymbol{s}))}\right)^2\right] \quad (4)$$

Where: l_c is a characteristic length which limits the domain of neighbouring points and $\rho(\boldsymbol{x}, \sigma_{prin}(\boldsymbol{s}))$ is a scalar which describes the interaction between points. It depends on the point location $\boldsymbol{x}$ and $\sigma_{prin}(\boldsymbol{s})$ the principal stress state on the surrounding point $\boldsymbol{s}$.

Therefore, the evolution of damage will depend on the non-local state variable:

$$d = d(Y^{nl}) \quad (5)$$

Seeing that, the damage starts above a threshold Y_0 ($d = 0$ for $Y^{nl} \leq Y_0$)) and cannot decrease, seeing that ($d \geq 0$).

In this paragraph, our objective is to provide a concise overview of the essential formulations of the three damage models employed in our numerical simulations. Furthermore, the non-local formulations associated to each model will be described briefly. It is important to note that this paragraph offers only a brief overview. For more comprehensive details, readers are encouraged to refer to the corresponding references cited in this paper.

Modified Von Mises model (MVM)

By introducing a state variable Y, as represented in Equation 6, De Vree *et al* (1995) developed a damage evolution law by employing the exponential Equation 7, as follows:

$$Y = \frac{k-1}{2k(1-2\nu)} I_1 + \frac{1}{2k}\sqrt{\left(\frac{k-1}{1-2\nu} I_1\right)^2 + \frac{12k}{(1+2\nu)^2} J_2} \quad (6)$$

$$d = 1 - \frac{Y_0(1 - B_2)}{Y^{nl}} - B_2 \exp\left[-B_1(Y^{nl} - Y_0)\right] \quad (7)$$

Where:

k = the ratio of compressive strength to tensile strength

I_1 and I_2 = respectively the first and the second invariant of the deviatoric strain tensor

B_1 = parameter associated to the slope at the peak of the stress-strain curve

B_2 = parameter associated to the residual strength

Y_0 = initial threshold of damage

ν = Poisson's ratio.

Mazars damage model

In this model (Mazars 1986) Y is defined as a function of the principal strains so that it is more sensitive to positive strains than to negative strains, as shown in Equation 8:

$$Y = \sqrt{\sum_i [\max(0, \varepsilon_i)]^2} \quad (8)$$

Equation 8 shows that only positive principal strains are considered in the definition of Y. In addition, and in order to represent the asymmetric fracture behaviour of concrete, Mazars (1986) proposes two damage variables: D_t in tension and D_c in compression. The linear combination of these two damage modes gives a global isotropic damage variable d such as:

$$d = \alpha_t d_t + \alpha_c d_c \quad (9)$$

With an exponential expression for the evolution of damage:

$$d_t = 1 - \frac{Y_0(1 - A_t)}{Y^{nl}} - A_t \exp[-B_t(Y^{nl} - Y_0)] \quad (10)$$

$$d_c = 1 - \frac{Y_0(1 - A_c)}{Y^{nl}} - A_c \exp[-B_c(Y^{nl} - Y_0)] \quad (11)$$

Where, in Equations 9, 10 and 11:

α_t and α_c represent weighting coefficients calculated from the strain tensor ε, as described in detail in Pijaudier-Cabot *et al* (1991), and Pegon and Anthoine (1997)

A_t and B_t = parameters for traction

A_c and B_c = parameters for compression.

It should be noted that the non-local calculations can be carried out in this model by substituting in Equations 10 and 11 the local state variable Y by the non-local one Y^{nl} obtained by using Equations 3 and 4.

RICRAG model

In this model, a state potential is introduced so that it takes into account elasticity, damage, sliding between cracked surfaces and hardenings as follows:

$$\rho\Psi = \frac{1}{2}\left\{\frac{\kappa}{3}[(1 - d)\langle\varepsilon_{kk}\rangle_+^2 - \langle-\varepsilon_{kk}\rangle_+^2) + 2(1 - d)\mu\varepsilon_{ij}^D\varepsilon_{ij}^D + 2d\mu(\varepsilon_{ij}^D - \varepsilon_{ij}^\pi)(\varepsilon_{ij}^D - \varepsilon_{ij}^\pi) + \gamma\alpha_{ij}\alpha_{ij}\right\} + \mathbf{H}(z) \quad (12)$$

The first and second terms (inside the brackets) of Equation 12 consist in coupling damage with elasticity, where ρ is the material density, κ and μ are the bulk and shear coefficients respectively, ε_{ij} is the second order total strain tensor, and ε_{ij}^D is the second order deviatoric total strain tensor, such as $\varepsilon_{ij}^D = \varepsilon_{ij} - \frac{1}{3}\varepsilon_{kk}\delta_{ij}$ where δ_{ij} is the second order Kronecker tensor. It should also be noted that the unilateral effect is taken into account by the separation of the total strain tensor into positive and negative parts, as shown in the first term. The symbol < > + denotes the positive part of the tensor. The third term $(2d\mu(\varepsilon_{ij}^D - \varepsilon_{ij}^\pi)(\varepsilon_{ij}^D - \varepsilon_{ij}^\pi))$ represents the contact sliding mechanism with friction where ε_{ij}^π is the second order sliding tensor.

Finally, the last terms $(\gamma\alpha_{ij}\alpha_{ij})$ and $\mathbf{H}(z)$ are introduced to take into account the part of the strain energy retained by friction and hardening energy rates. Both kinematic and isotropic hardenings are considered; γ is a material parameter, α_{ij} the second order tensor associated to the kinematic hardening, z the internal variable related to the isotropic hardening and $\mathbf{H}$ the consolidation function.

After development by Richard *et al* (2010), the first state equation (Equation 13) can be deduced:

$$\sigma_{ij} = \frac{\partial\rho\Psi}{\partial\varepsilon ij} = \frac{\kappa}{3}[(1 - d)\langle\varepsilon_{kk}\rangle_+ - \langle-\varepsilon_{kk}\rangle_+)\delta_{ij} + 2(1 - d)\mu\varepsilon_{ij}^D + 2d\mu(\varepsilon_{ij}^D - \varepsilon_{ij}^\pi) \quad (13)$$

A threshold surface denoted f_d is introduced:

$$f_d = Y - (Y_0 + Z) \text{ so that } \dot{d} = \dot{\lambda}_d \cdot \frac{\partial f_d}{\partial Y} \quad (14)$$

Where: $\dot{\lambda}_d$ is a Lagrange multiplier and Z a thermodynamic force associated with isotropic hardening:

$$Z = \frac{\partial\rho\Psi}{\partial z} = \frac{\partial\mathbf{H}(z)}{\partial z} \quad (15)$$

In Equation 14, Y denotes the energy variable driving damage and Y_0 an initial threshold. This variable Y is defined through the decomposition between direct extension mechanisms (tension) and induced extension mechanisms (compression):

$$Y = \beta Y_{Dir} + Y_{Ind} \quad (16)$$

with

$$Y_{Dir} = \frac{1}{2}\varepsilon_{ij}^{Dir}E_{ijkl}\varepsilon_{kl}^{Dir} \quad (17)$$

$$Y_{Ind} = \frac{1}{2}\varepsilon_{ij}^{Ind}E_{ijkl}\varepsilon_{kl}^{Ind} \quad (18)$$

Where: E_{ijkl} is the fourth order Hooke tensor computed from the elastic parameters κ and μ, and β is a parameter driving the dissymmetry of the threshold surface between tension and compression. The direct and induced extensions tensors are obtained through the following decompositions (H is the Heaviside function):

$$\varepsilon_{ij}^{Dir} = \langle\varepsilon_{ij}\rangle_+ H(\langle\varepsilon_{ij}\rangle_+\langle\sigma_{ij}\rangle_+) \quad (19)$$

$$\varepsilon_{ij}^{Ind} = \varepsilon_{ij} - \varepsilon_{ij}^{Dir} \quad (20)$$

For the non-local calculations, the local damage energy released rate Y is replaced by the non-local one Y^{nl} obtained by using Equations 3 and 4, so that the damage threshold surface becomes:

$$f_d^{nl} = Y^{nl} - (Y_0 + Z) \text{ and } \dot{d} = \dot{\lambda}_d \cdot \frac{\partial f_d}{\partial \bar{Y}^{nl}} \quad (21)$$

Finally, the expression of the damage variable can be written:

$$d = 1 - \frac{1}{1 + (A_{Dir}H(\langle\varepsilon_{ij}\rangle_+\langle\sigma_{ij}\rangle_+) + A_{Ind}(1 - H(\langle\varepsilon_{ij}\rangle_+\langle\sigma_{ij}\rangle_+)))(Y^{nl} - Y_0)} \quad (22)$$

Where: A_{Dir} and A_{Ind} are the material parameters which can be interpreted as brittleness terms, respectively, in tension and in compression.

DESCRIPTION OF THE DAM AND ITS NUMERICAL MODELLING

The Beni-Haroun gravity dam, depicted in Figure 1 (see page 3), is situated in a seismic zone in north-eastern Algeria. It is widely recognised as one of the most important dams in Africa, and the largest dam in Algeria in terms of storage capacity, with a capacity of 960 million cubic metres. The dam is founded on a limestone rock foundation. The maximum height and base width of the dam are 118.4 m and 92.05 m, respectively. The dam crest is 8 m wide, and the maximum height of the reservoir water is considered as 102.1 m.

Material properties

The material properties, for both the concrete gravity dam and the foundation, are the same as those described in Si-Chaib *et al* (2018), and are listed in Table 1.

In addition to Young's modulus and the Poisson's ratio, each damage model used in this study requires the knowledge of five parameters. Indeed, for the Modified Von Mises (MVM) model, the material properties were taken as follows:

B_1 = 13 000, B_2 = 0.5, $Y_0 = 10^{-4}$ and k = 10.

For the Mazars model, the material properties were taken as follows:

A_t = 1, A_c = 1.4, $Y_0 = 10^{-4}$, B_t = 15 000 and B_c = 1 900.

And for the RICRAG model, the set of material properties were taken as:

$F_t = 3.6 \times 10^{+6}$ Pa, $A_{Dir} = 10^{-2}$ J.m^{-3}, $\alpha_0 = A_{Ind} = 9 \times 10^{-5}$ J.m^{-3}, $\alpha_0 = 2 \times 10^{-7}$ Pa^{-1} and $\gamma_1 = 7 \times 10^9$ Pa.

For the contact approach, Coulomb's friction law was used, with a coefficient of friction taken equal to 0.84 which is the same value as adopted in the study performed in Si-Chaib *et al* (2018).

Finite elements model of the dam foundation system

The dam foundation system was modelled according to the geometrical layout shown in Figure 2 (see page 4). The soil domain assumes a rectangular shape, measuring 292.05 m in width and 100 m in depth. As previously mentioned, an inclined stepped abutment with a height of 4 m was constructed at the foundation interface using earthwork techniques.

The dam is subjected to progressive pushover loading, with a uniform acceleration gradually increasing from 0.15 g with a constant increment of 0.05 g until reaching an intensity of 0.7 g for the contact model, with interface and a limit intensity of 1.25 g for the continuous model without joint. Consequently, for the model incorporating the interface, twelve load steps are employed, while the model without the joint utilises twenty-two load steps. Beyond these limit values of 0.7 g and 1.25 g, calculations exhibit significant divergence due to instabilities and subsequent failure mechanisms.

The hydrodynamic effects of the stored liquid are modelled using added masses at the upstream dam face, following Westergaard's approach (Westergaard 1933), given as follows:

$$m(z) = \frac{7}{8}\rho_w\sqrt{H_w(H_w - h)} \qquad (23)$$

Where: ρ_w is the water density, H_w is the reservoir height and h is the height coordinate measured from the base of the dam.

Figure 3 displays the envelope curve of maximum values, which represents the most unfavourable profile of uplift pressures. These measurements were taken from the most critical profiles reported in the works of Si-Chaib *et al* (2018). The boundary conditions and pressure loads are illustrated in Figure 4.

A two-dimensional plane strain finite element model, comprising 9 239 four-node quadrilateral (QUA4) elements, was employed to simulate the dam-rock foundation structure, as depicted in Figure 5. These calculations were performed using the Cast3M code developed by the CEA in France (Cast3M 2023).

Furthermore, to conduct non-local calculations, it is essential for the mesh size of the elements of the dam to be smaller than the characteristic length of the concrete l_c, as earlier introduced in Equation 4. In addition, according to Bažant and Pijaudier-Cabot

Table 1 Material properties of Beni-Haroun Dam

Material	Material properties		
	Elasticity modulus (Pa)	Poisson's ratio	Mass density (Kg/m^3)
Concrete dam	30 000.10^6	0.2	2 350
Foundation	15 000.10^6	0.33	2 100

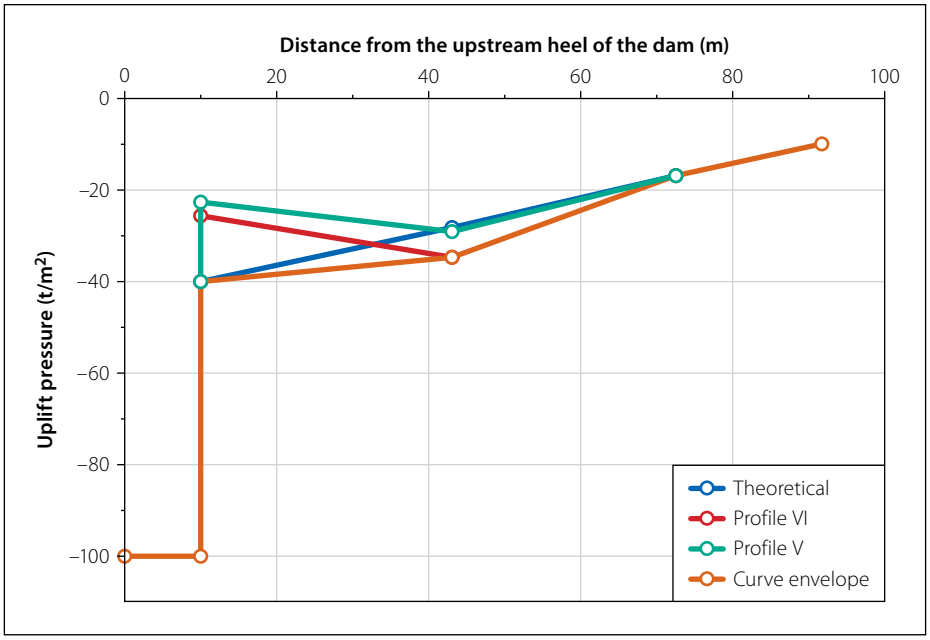

Figure 3 The curve envelope of the maximum values obtained from the theoretical profile and profiles V and VI

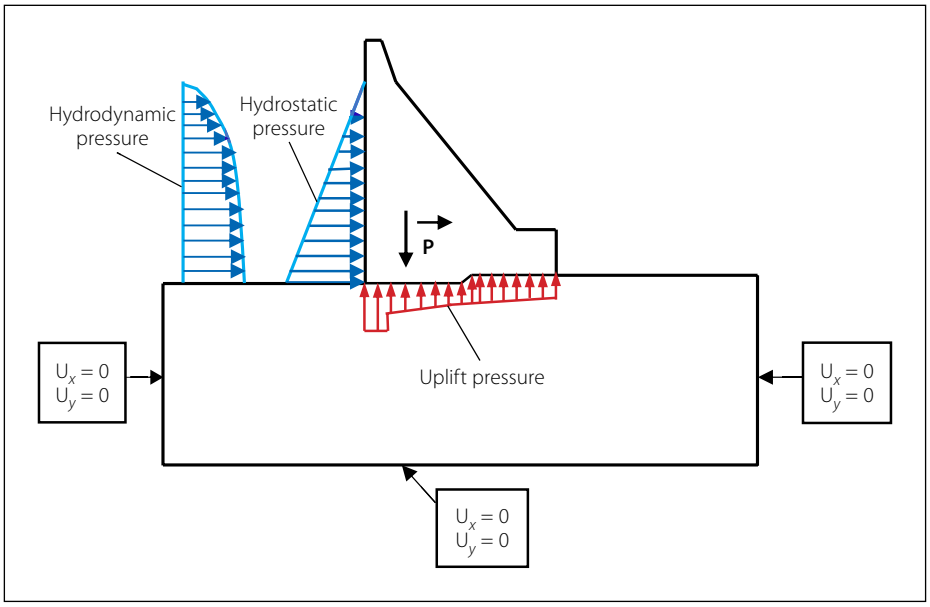

Figure 4 Pressure loads and boundary conditions

(1989), this characteristic length is comprised between 3 d_a and 5 d_a, where d_a represents the maximum aggregate size of concrete. In other words, this characteristic length must exceed the size of the mesh elements in regions where damage is likely to occur and propagate. For this purpose, considering a maximum aggregate size of 150 mm, a value of *lc* can be chosen as equal to 600 mm.

The contact simulation utilised compatible meshes in which every pair of nodes facing each other is positioned at the same location on the interfaces in their initial state before applying loads. For this purpose, a one-dimensional linear element with two nodes was chosen as the contact element.

The seismic forces are applied at the finite element nodes of the dam proportionally to their assigned masses and applied acceleration. The calculation procedure is as follows:

$$\{F_I\} = [M]\{I_X\}.k.g$$

Where:

$[M]$ is the assembled mass matrix of the FE model

$\{I_X\}$ is the influence vector allowing to apply horizontal accelerations to all the nodes of the mesh so that:

$\{I_X\} = \{1\ 0\ 1\ 0\ \ldots\ 1\ 0\}^T$

k represents the fraction of gravity acceleration g.

In order to determine the mass *mi* at each node *i*, Consistent Mass Method was used. Compared to Lumped Mass Method, this approach ensures a more accurate representation of mass distribution by taking into account the shape functions used in finite element formulation. For an element with density ρ, volume V_e and shape function matrix $[N]$, the mass matrix $[Me]$ is:

$$[M_e] = \int_{Ve} \rho [N]^T [N] dV$$

Furthermore, hydrodynamic effects are incorporated by adding inertia forces corresponding to equivalent added masses at the upstream face nodes, due to the impounded water. Within the progressive pushover analysis, the seismic forces are calculated for each loading increment. This is achieved by multiplying the corresponding nodes masses with the associated seismic acceleration value. Furthermore, based on residual equilibrium forces, the convergence criteria for this non-linear analysis have been set to 10^{-4}.

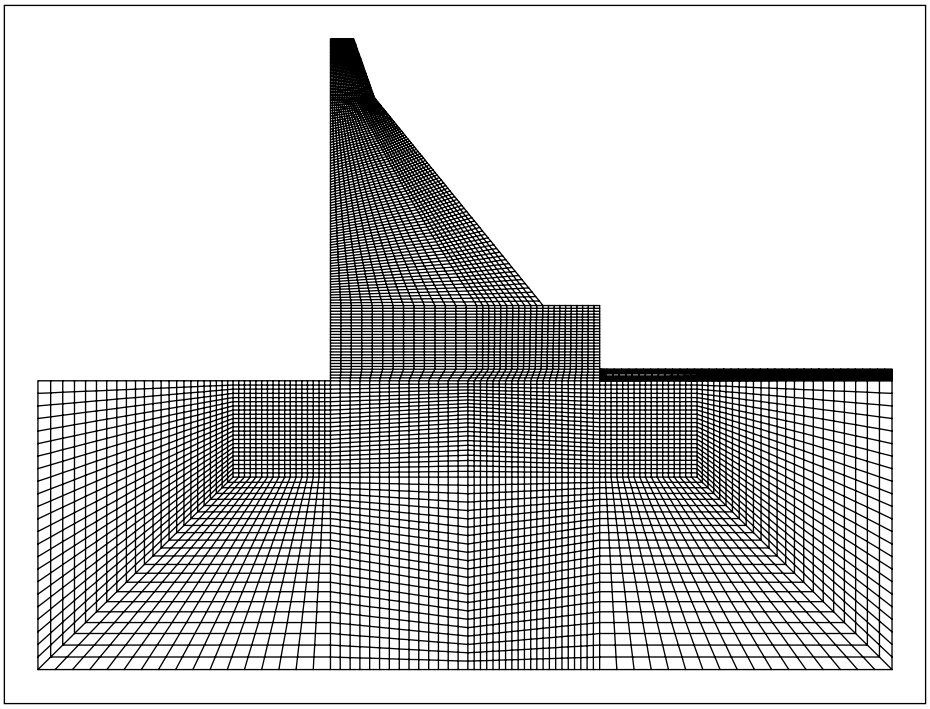

Figure 5 Adopted meshes for the dam-foundation system

RESULTS AND DISCUSSION

Damage analysis

The first part of this section aims to examine the effects of taking into account

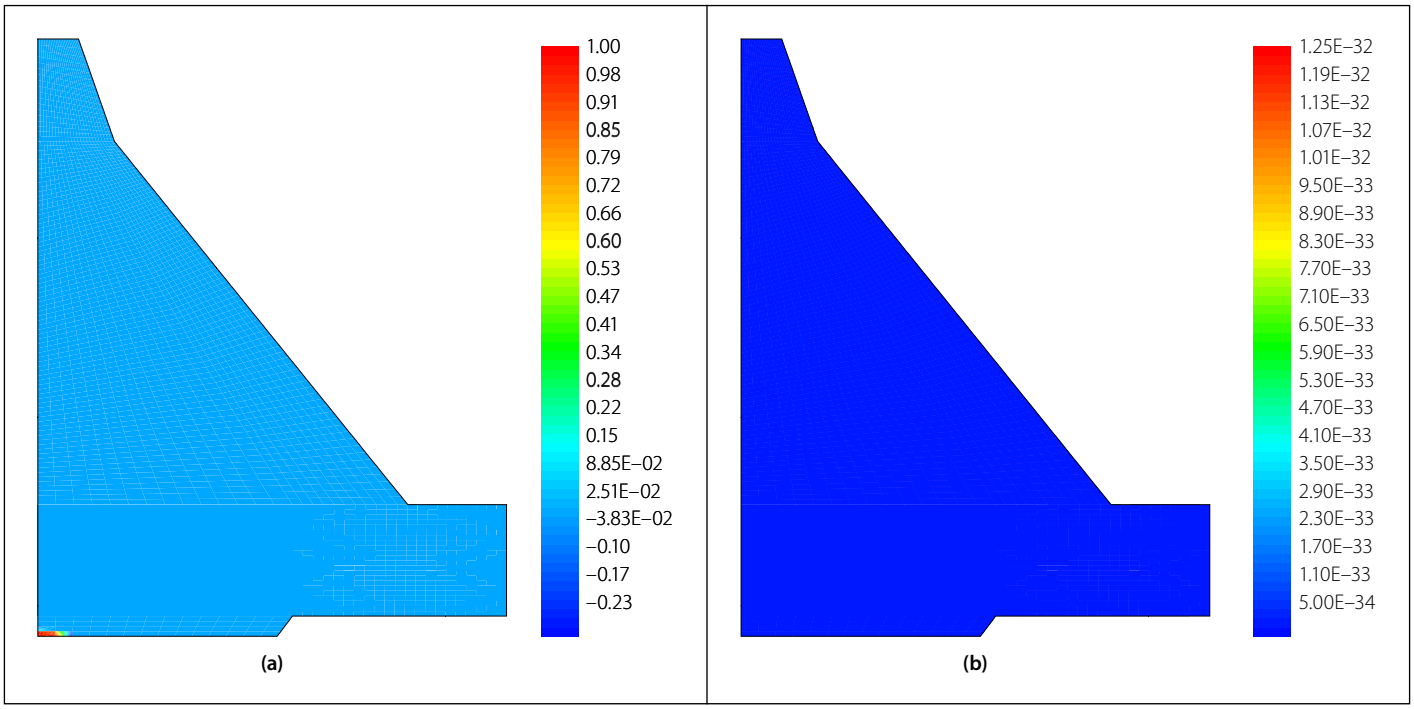

Figure 6 Damage distributions with the RICRAG damage model for 0.3 g: (a) without interface, (b) with joint

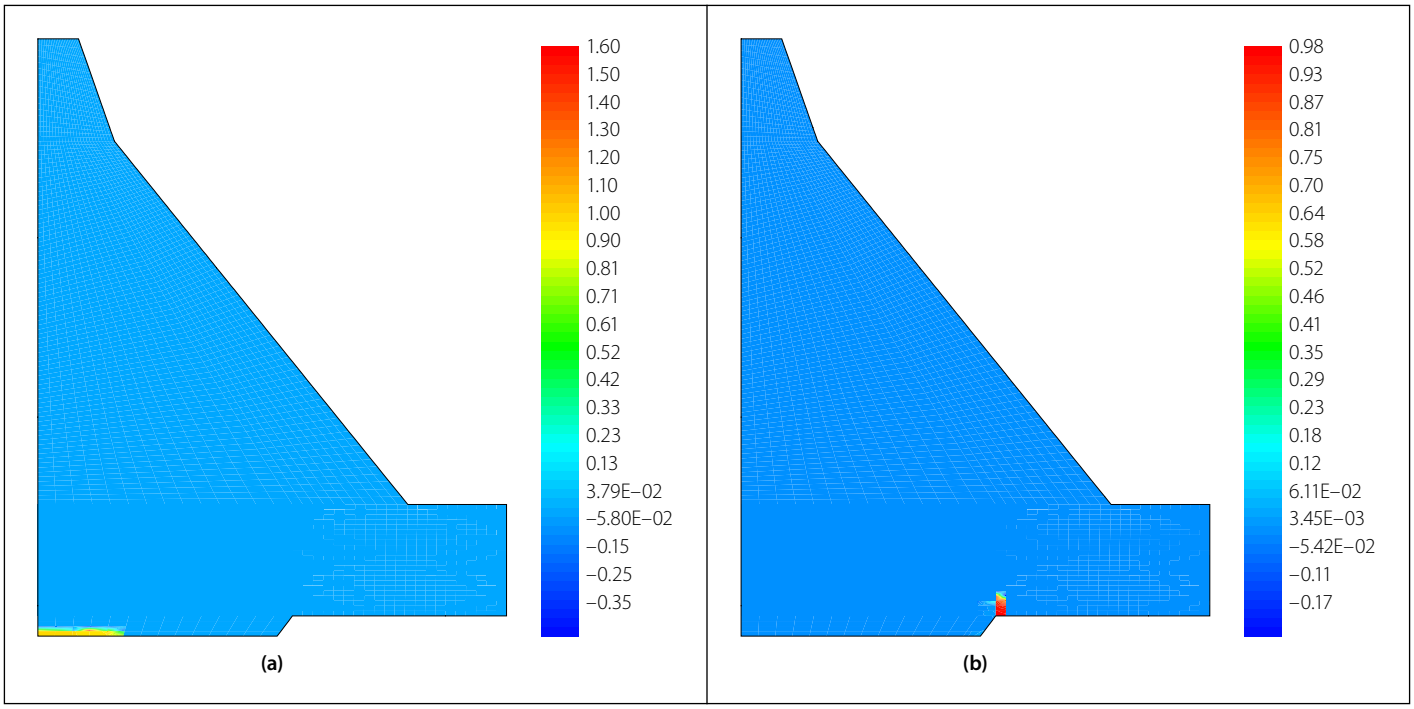

Figure 7 Damage distributions with the RICRAG damage model for 0.5 g: (a) without interface, (b) with joint

the dam-foundation contact conditions on the seismic damage behaviour. As a first step, the investigation will be limited to a simulation using the RICRAG damage model under pushover analysis. The choice of this model is based on its ability to take into account more phenomena, such as elasticity, plastic hardening, damage and sliding between cracked surfaces. Furthermore, numerical experiments have confirmed its effectiveness and robustness (Becheur *et al* 2018). For this purpose, and as mentioned earlier in the introduction, two calculation models will be studied. The first calculation model depicts the dam-foundation system with a continuous mesh, excluding consideration of interfaces. The second model addresses the dam-foundation contact problem, accounting for both contact conditions and frictions.

Considering three different acceleration magnitudes, specifically 0.3 g, 0.5 g, and 0.7 g where 'g' represents the acceleration due to gravity, Figures 6, 7 and 8 illustrate the corresponding damage distributions and their evolutions obtained from both calculation models. These figures clearly demonstrate that, in the contactless model, damage initiates at the heel (upstream base) of the dam and propagates horizontally as acceleration increases. In the second model, damage occurs at the dam's abutment and progresses vertically with increasing acceleration. Notably, it is observed that the initiation of damage is delayed in the second model with interface, while damage occurs significantly earlier in the first model without joint.

To further validate the previous results, the second part of our calculations involves a comparative analysis of damage distributions obtained from the RICRAG model

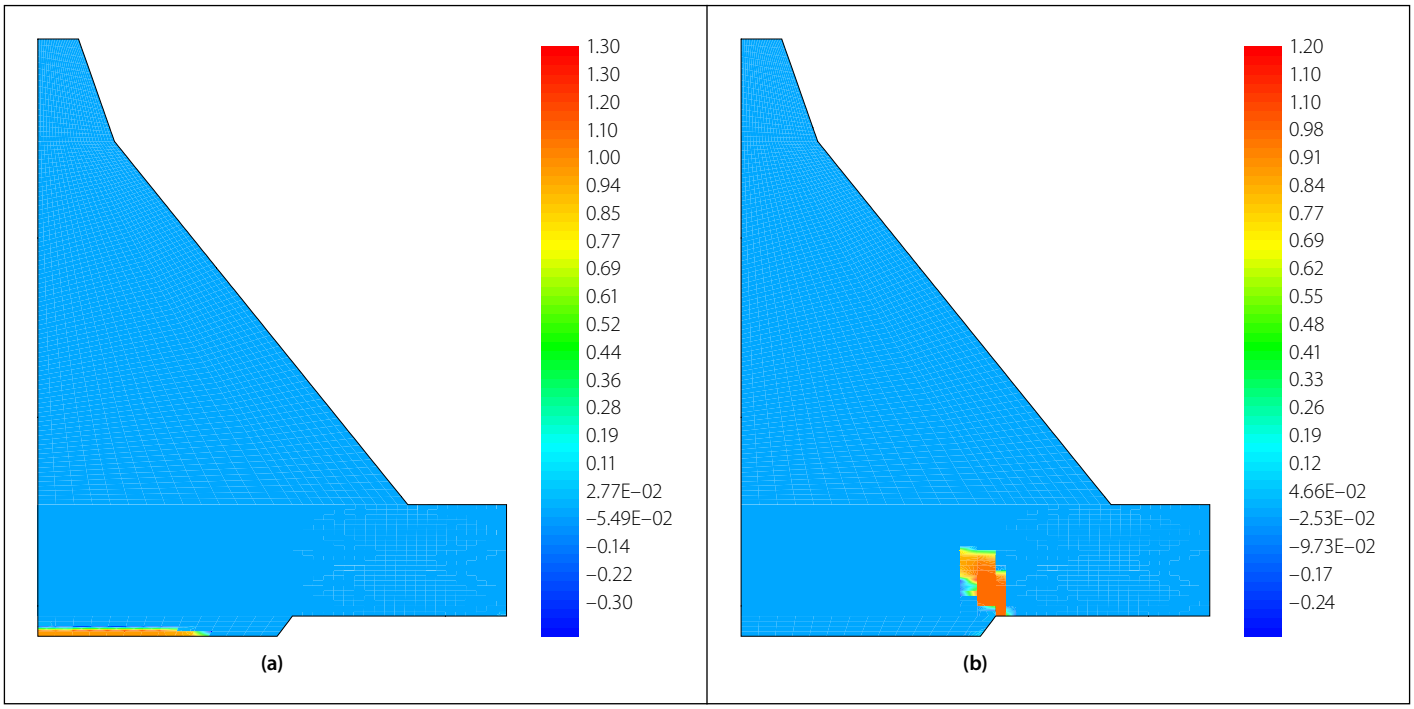

Figure 8 Damage distributions with the RICRAG damage model for 0.7 g: (a) without interface, (b) with joint

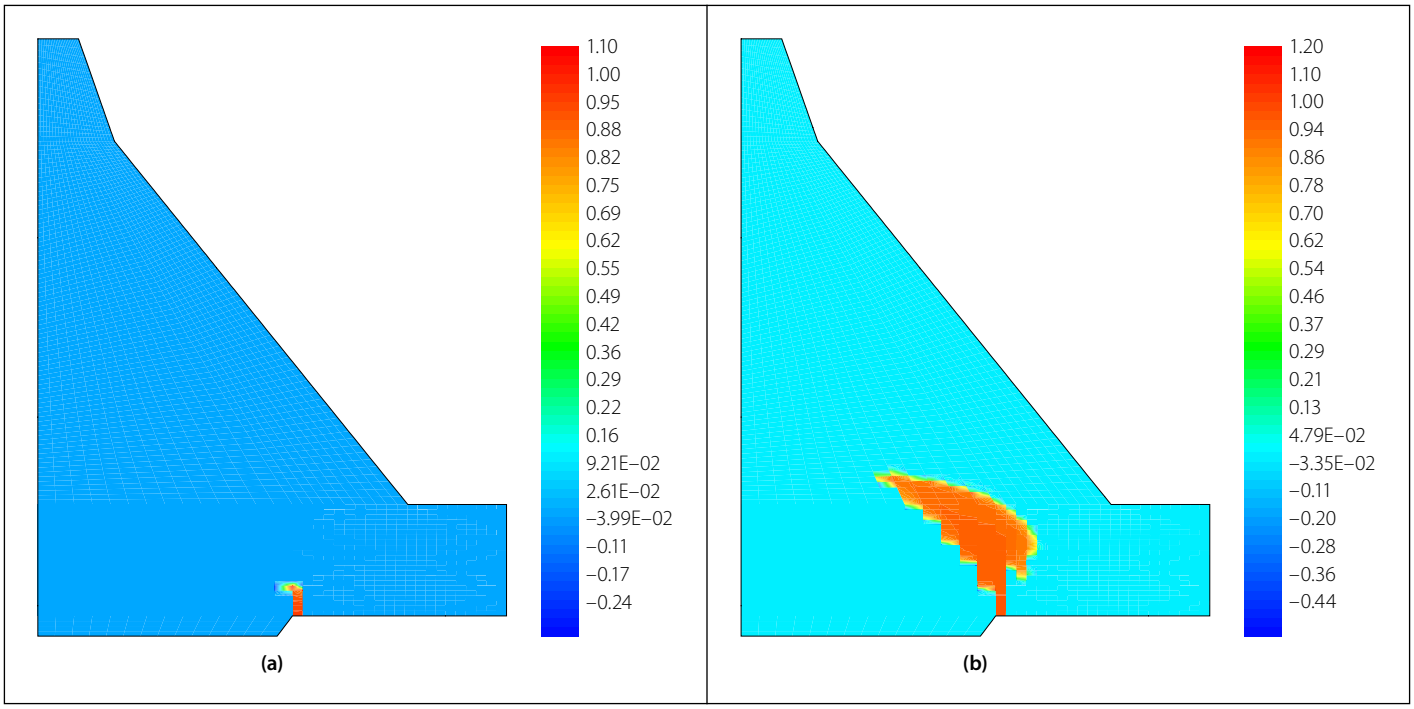

Figure 9 Damage distributions with the MVM damage model: (a) for 0.5 g, (b) for 0.7 g

against two other models, namely, MVM and Mazars. Specifically, focusing solely on the contact model under the effects of two different magnitudes, 0.5 g and 0.7 g, Figures 9, 10 and 11 illustrate the distribution of damage fields and their progressions.

These figures reaffirm the observation that damage initiates near the dam's abutment and propagates as acceleration increases. Furthermore, it becomes evident that, for the same magnitude, the dam experiences more extensive damage when using the Mazars model compared to the others.

Stress analysis

Regarding the distribution and evolution of stress fields, our analysis focused primarily on the examination of the principal stresses obtained using the RICRAG model. For this purpose Figures 12, 13 and 14 respectively depict the isovalue representations of principal stresses within the rock foundation-dam structure for the same magnitudes as considered previously. By examining these figures, it can be discerned that for a magnitude of 0.3 g, the tensile stresses, which appear to be the primary cause of damage, are notably lower in the second model with interface (compare Figure 12(b) with 12(a)). However, as the magnitude increases, these tensile stresses with the same model with joint become significantly higher (compare Figures 13(b) and 14(b) with Figures 13(a) and 14(a) respectively). Specifically, at a lower magnitude of 0.3 g, they approach a value of 4 MPa in Figure 12(b) and are distributed along the interface. In contrast, in the case of the continuous mesh of Figure 12(a), and under the same magnitude (0.3 g), these tensile stresses are distinctly concentrated in the vicinity of the singularity zone at the

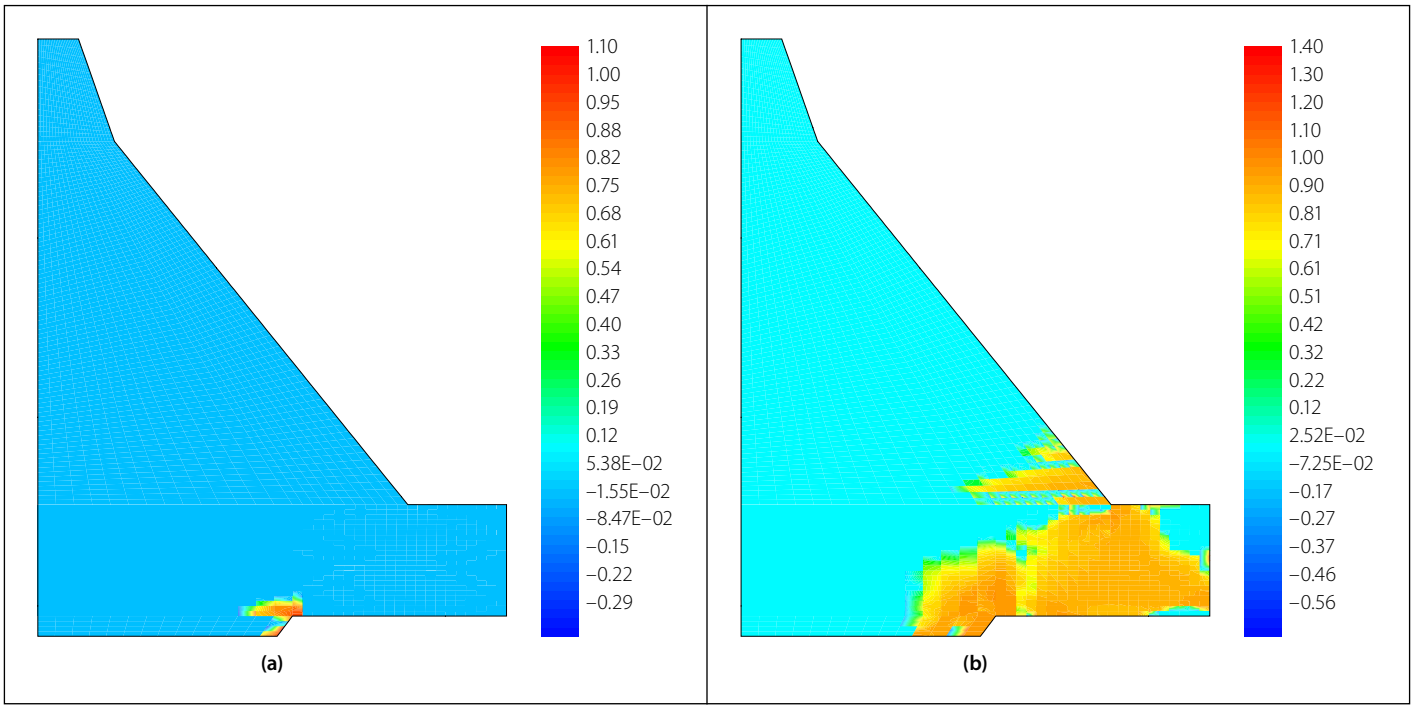

Figure 10 Damage distributions with the MAZARS damage model: (a) for 0.5 g, (b) for 0.7 g

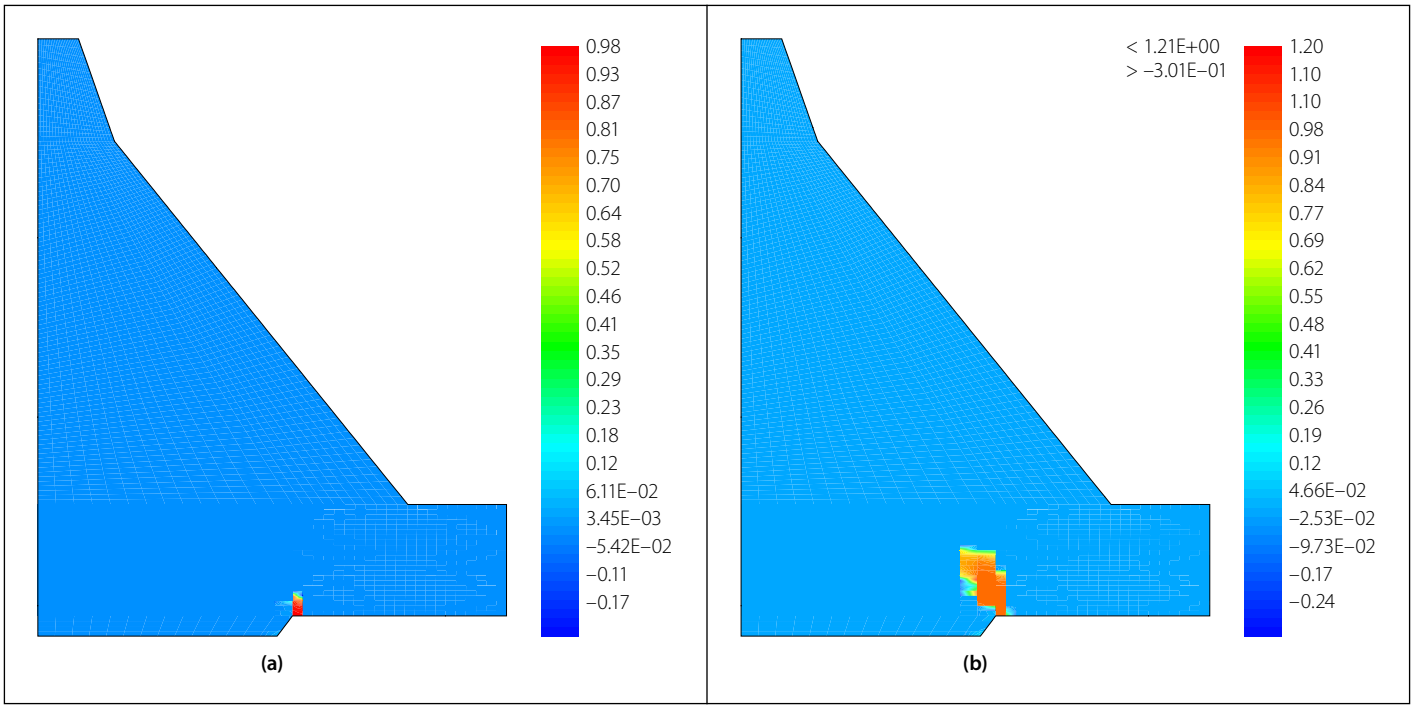

Figure 11 Damage distributions with the RICRAG damage model: (a) for 0.5 g, (b) for 0.7 g

heel and rapidly reach maximum values of 6 MPa.

The augmentation of tensile stresses in the model with joints for magnitudes of 0.5 g and 0.7 g can be explained by the partial separation and sliding occurring at the interface, followed by a stress redistribution that concentrates stresses in the steep gradient zone of the foundation abutment, which experiences increased stresses. Indeed, for these same magnitudes, the maximum values of these tensile stresses reach approximately 20.7 (Figure 13(b)) and 27.6 MPa (Figure 14(b)), in contrast to 6.42 MPa (Figure 13(a)) and 8.87 MPa (Figure 14(a)) in the case without joint. Nevertheless, it's worth noting that these elevated values can be significantly reduced by replacing sharp corners with fillets as stipulated by the rules of good construction. Another way to mitigate these issues is by opting for an elastoplastic behaviour model for the foundation soil as demonstrated in Durieux and Van Rensburg (2016), rather than the elastic model adopted in this paper.

The preceding results prompted the authors to investigate the principal stress distributions within the dam considered separately to improve the understanding thereof. Figures 15, 16 and 17 depict these stress fields and their evolutions under the influence of the same magnitudes. Comparing the results in Figures 12(b), 13(b) and 14(b) to those in Figures 15(b), 16(b) and 17(b) reveals that the principal tensile stresses within the dam, as provided by the calculation model with interface, are considerably lower. Specifically, Figures 12(b), 13(b) and 14(b) respectively show maximum values of 4.03, 20.7 and 27.6 MPa, while the dam, considered separately, exhibits values of 2.83 MPa, 5.73 MPa and 5.49 MPa. This suggests that the high tensile stress values of 20.7 and 27.6 MPa are associated with points belonging to the foundation mass rather than the dam itself, indicating that the dam is under less stress and in a less critical condition.

However, when comparing the results obtained from the two calculation models, with and without joint, as shown in Figures 15(b), 16(b) and 17(b) against Figures 15(a), 16(a) and 17(a), the phenomena of partial separation and sliding at the interface followed by stress redistribution and concentration as mentioned in the previous paragraph is confirmed. Indeed, for lower magnitudes, the contact approach yields relatively lower values (around

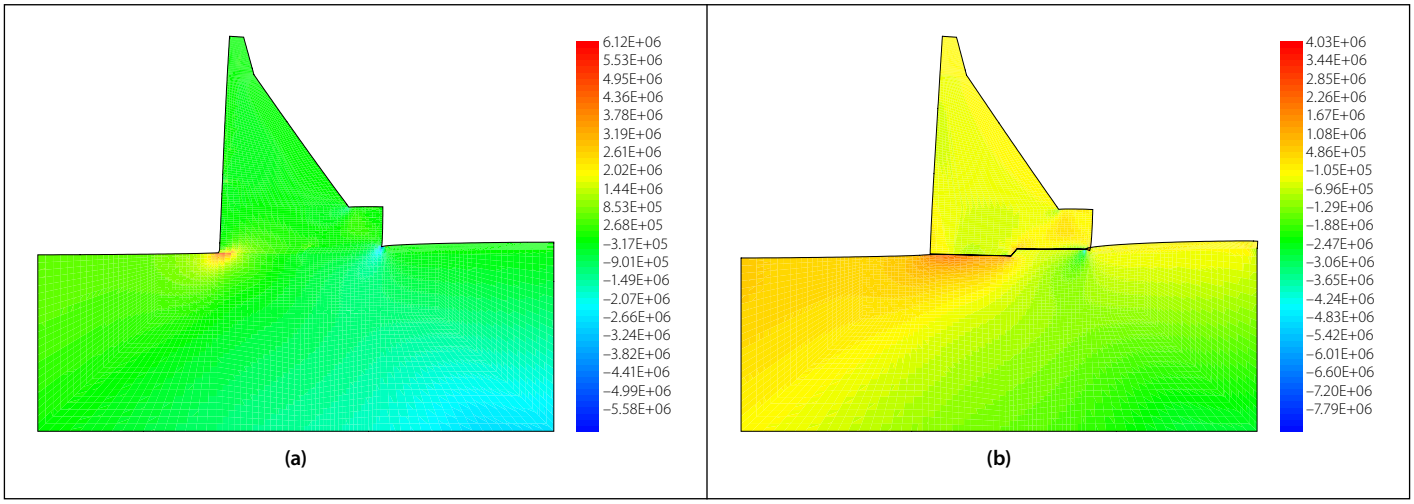

Figure 12 Principal stress isovalues with the RICRAG damage model for 0.3 g: (a) without, (b) with interface

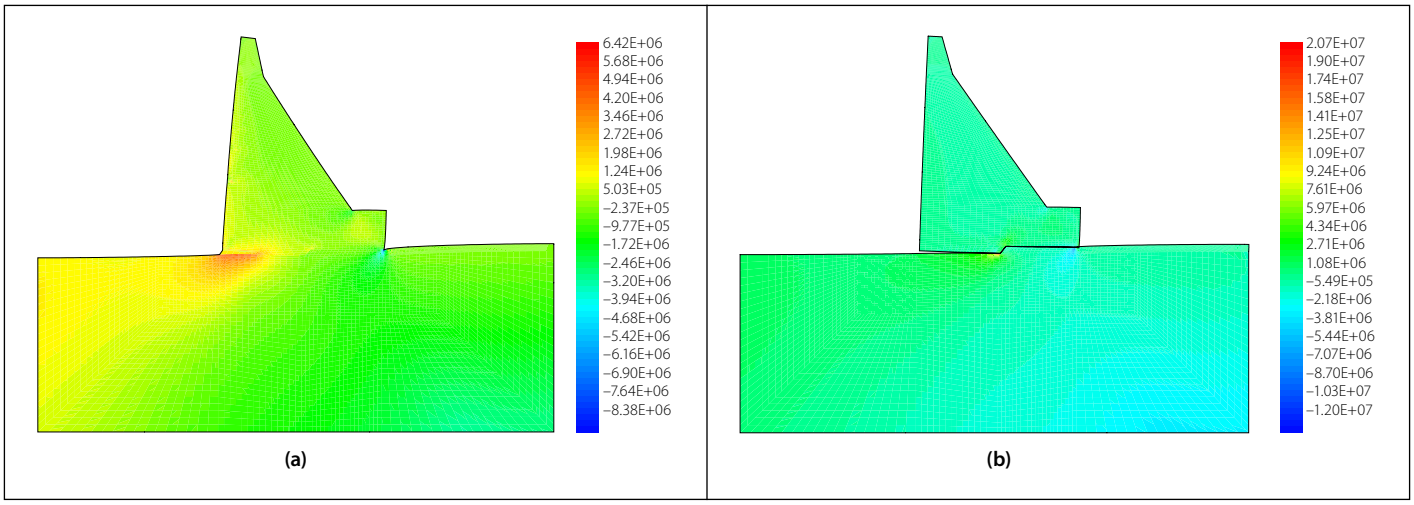

Figure 13 Principal stress isovalues with the RICRAG damage model for 0.5 g: (a) without, (b) with interface

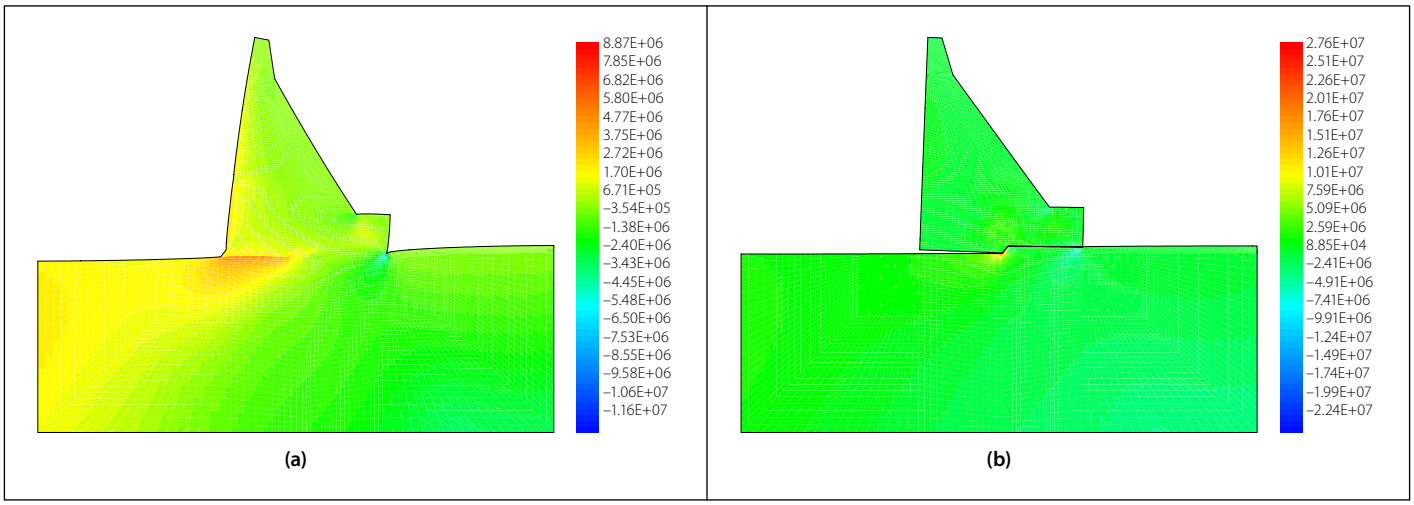

Figure 14 Principal stress isovalues with the RICRAG damage model for 0.7 g: (a) without, (b) with interface

2.83 MPa), compared to 3.89 MPa in the contactless model. Conversely, under magnitudes of 0.5 g and 0.7 g, the stresses are notably higher, reaching values of 5.73 and 5.49 MPa, respectively, compared to 3.71 and 4.61 MPa (as seen in Figures 16 and 17). This is also confirmed by the evolution of the computed nodal reactions of the lower contact surface represented in Figure 18 for

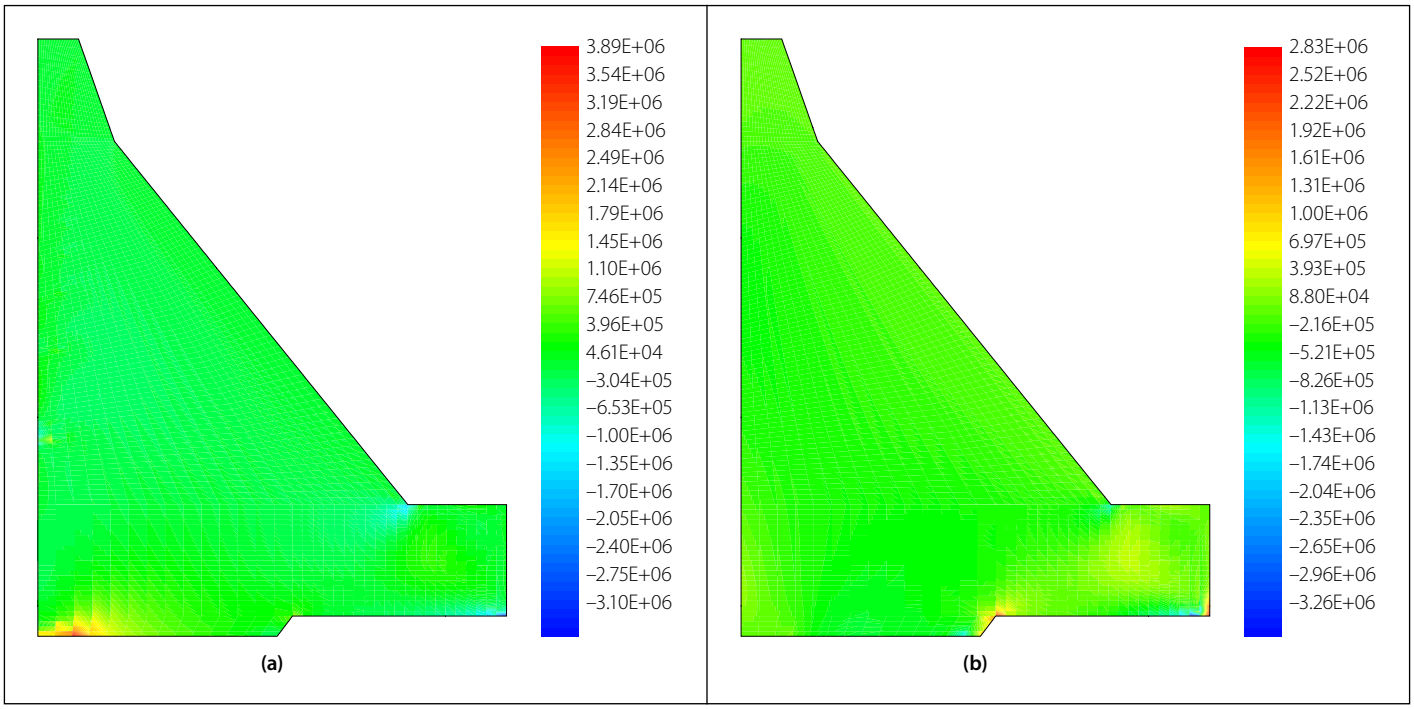

Figure 15 Principal stress isovalues with the RICRAG damage model for 0.3 g: (a) without, (b) with interface

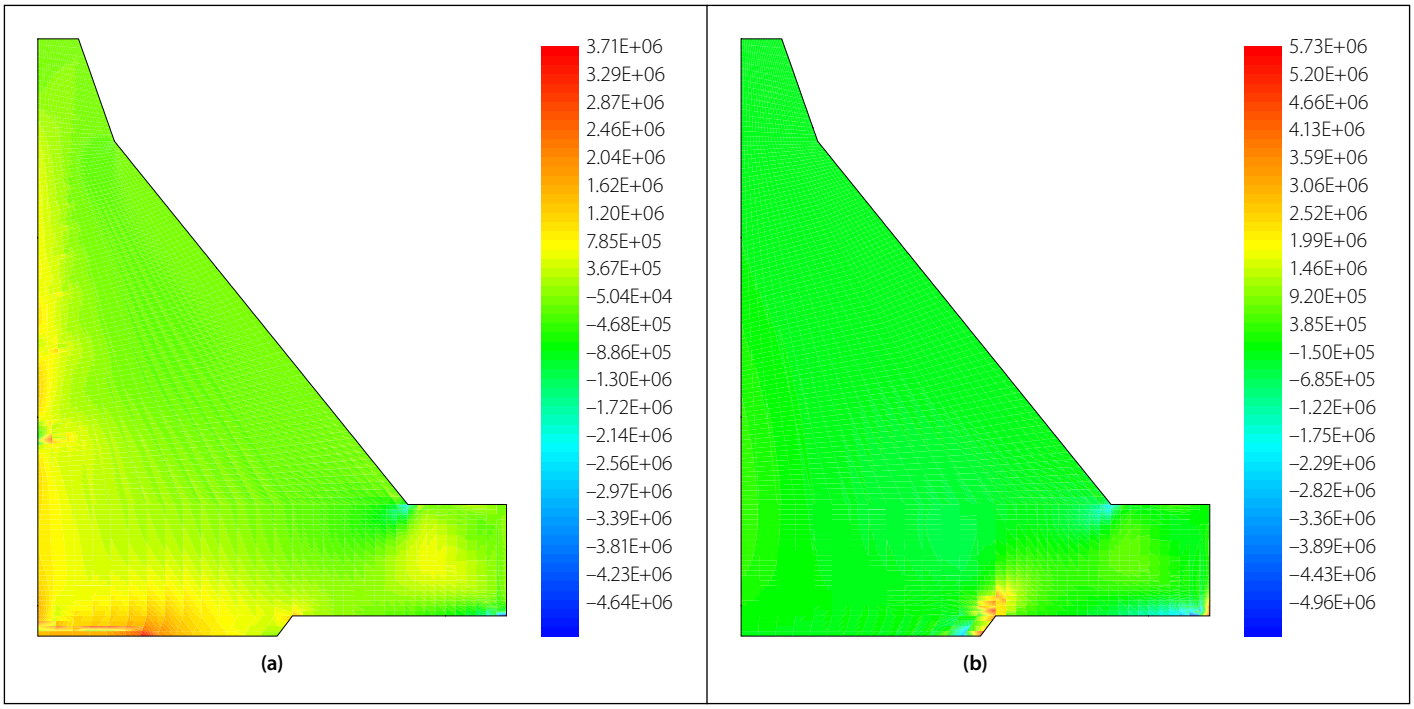

Figure 16 Principal stress isovalues with the RICRAG damage model for 0.5 g: (a) without, (b) with interface

the initial case (without seismic actions), and subsequently for the magnitudes of 0.15 g, 0.3 g, 0.5 g, 0.6 g and 0.7 g.

Review of displacement results obtained

Figures 19 and 20 represent the evolutions of the horizontal and vertical displacements at the crest as a function of the magnitudes of the intensities of the pushover action obtained from the two calculation models. For magnitudes up to 0.45 g, the horizontal displacement component values are closely matched (Figure 19). However, beyond this threshold, the disparity progressively grows, reaching 11 cm, where the model without interface records a horizontal displacement of 9.19 cm, while the model with joint reports a value of 19.9 cm. Regarding the vertical displacement components in Figure 20, they are nearly identical when the magnitude remains below 0.45 g. However, for higher magnitudes, discrepancies between the values grow, culminating in a 5.74 cm difference. This corresponds to a value of 6.78 cm for the model with interface and 1.14 cm for the model without joint. It should be noted that the negative values of the vertical components obtained by both models result from the instantaneous deformation of the rock foundation, which is subsequently compensated for by the positive contribution arising from the rotational movement of the dam.

In order to have a better knowledge of the overall response obtained by the RICRAG model, the simultaneous depiction of three curves was found to be useful. These curves correspond to the horizontal components of displacements at the crest obtained by the model with interface using

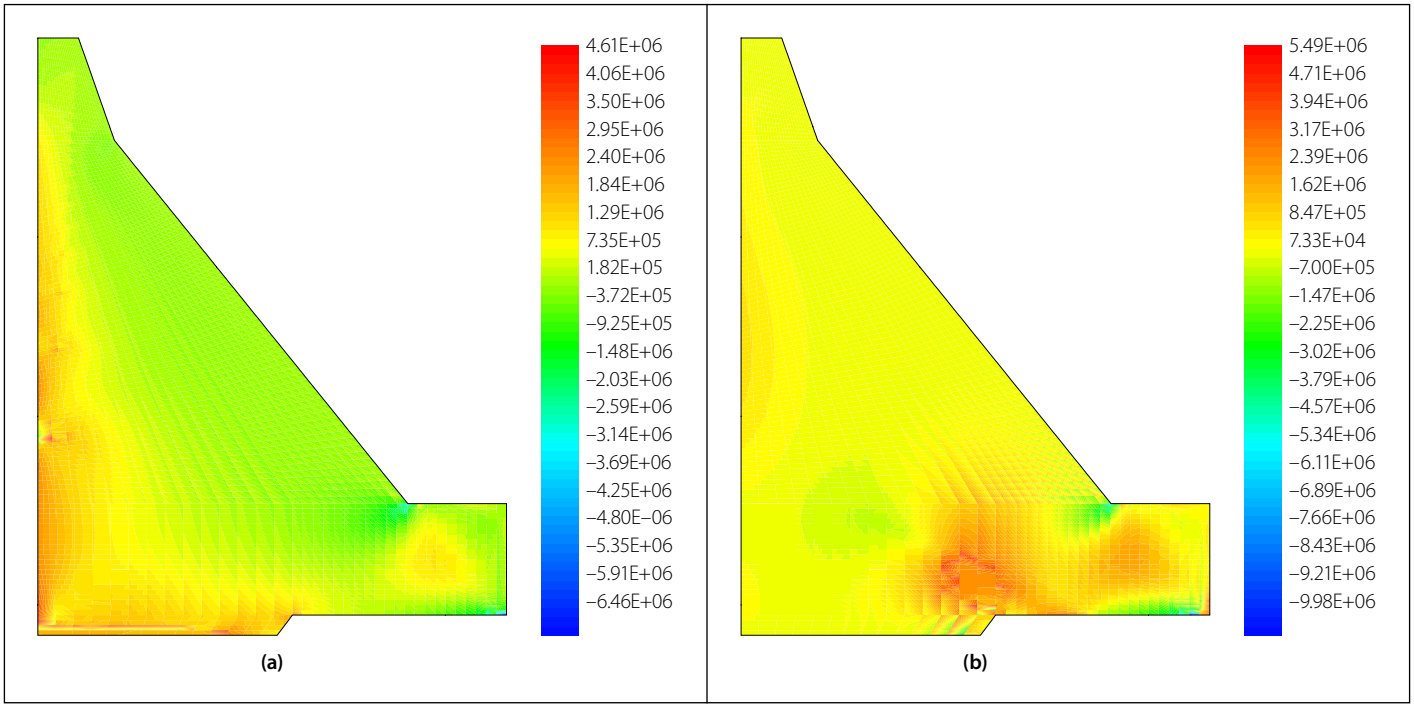

Figure 17 Principal stress isovalues with the RICRAG damage model for 0.7 g: (a) without, (b) with interface

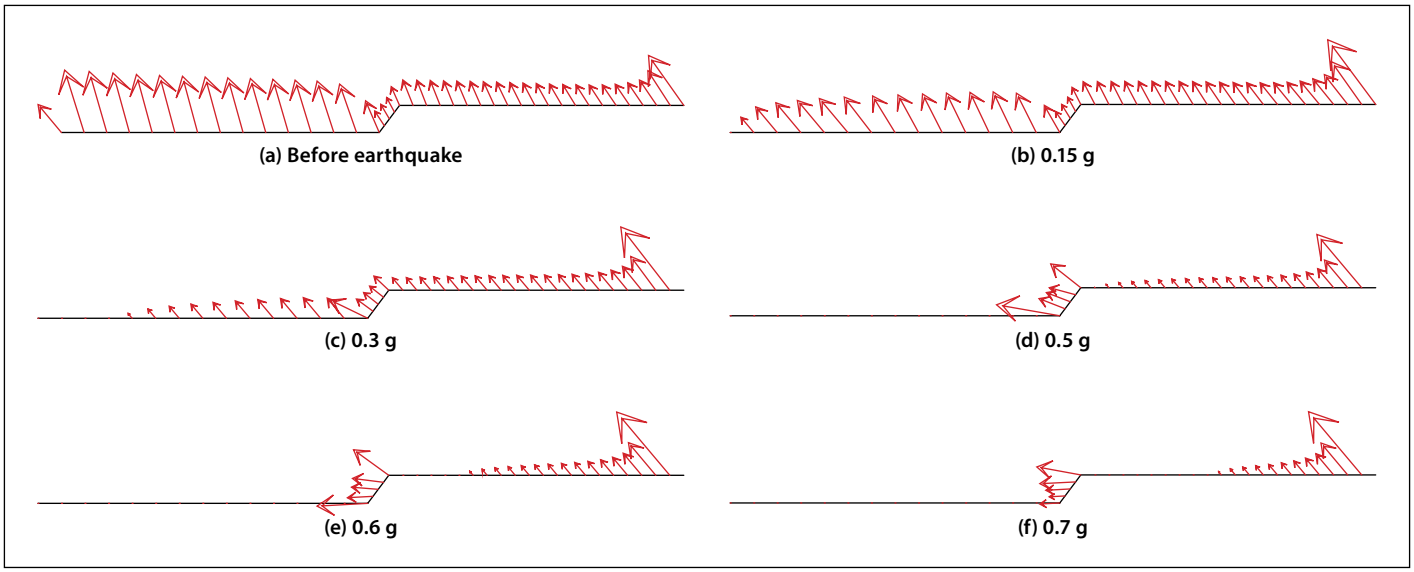

Figure 18 Evolution of the computed nodal reactions of the lower contact surface under progressive pushover actions

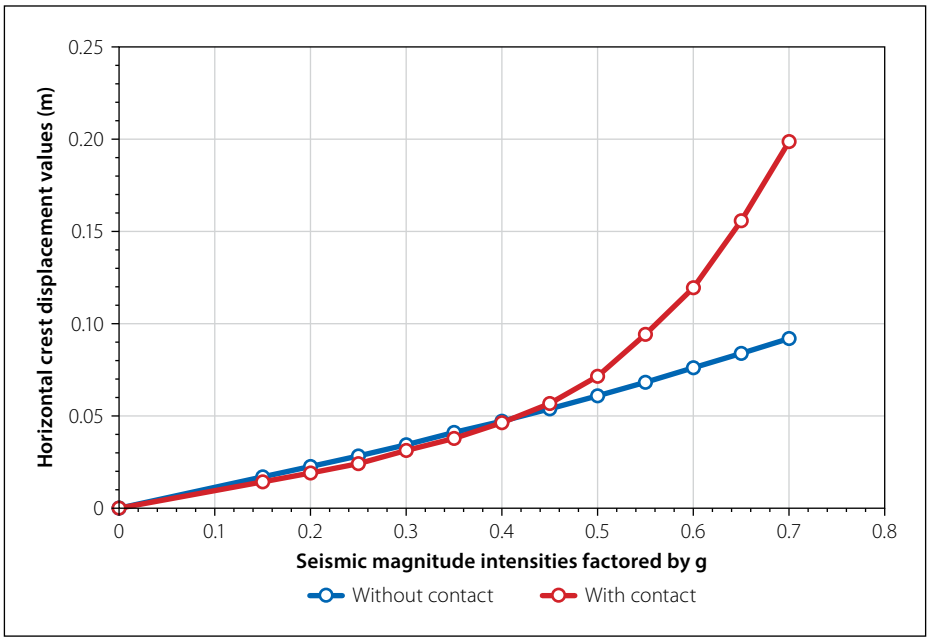

Figure 19 Horizontal crest displacement as a function of pushover action

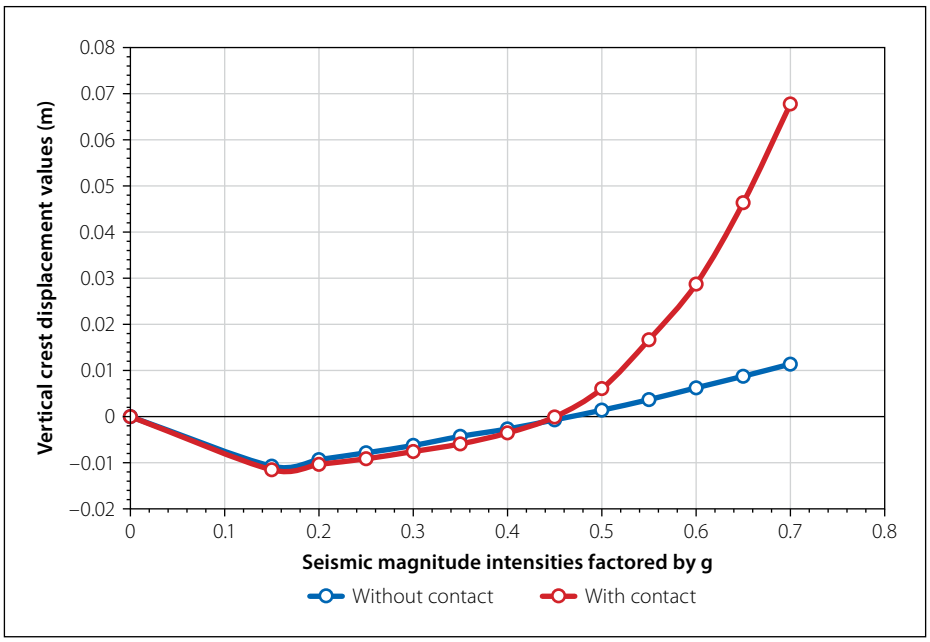

Figure 20 Vertical crest displacement as a function of pushover action

the three damage models. Indeed, Figure 21 shows that, for accelerations ranging from 0.15 g to 0.55 g, the obtained values are very close. However, for accelerations higher than 0.55 g, the analysis reveals discrepancies in the measured horizontal displacements. The results obtained by the Mazars damage model are less favourable, with values potentially leading to the failure of the dam reaching up to 135 cm under 0.7 g. In contrast, for the same magnitude, the MVM model provides a value of 35.1 cm, while the RICRAG model yields 20 cm.

Seismic capacity analysis

The seismic capacity of a structure refers to its inherent ability to resist earthquake forces. This capacity is quantified by the structure's strength, which represents the maximum resistance (reaction) it can develop against a given level of seismic demand (imposed response). In the context of gravity dams, this resistance is typically expressed as the total shear force at the base, while the imposed response is the displacement demanded at the dam crest due to seismic excitation. Evaluating this capacity is often achieved through static pushover analysis. In order to gain valuable insights into the dam's seismic response, particularly the influence of damage models and foundation assumptions on overall performance and energy dissipation, capacity curves are presented in Figure 22. An analysis of these curves reveals that all models exhibit comparable seismic capacities under low seismic demand conditions. This is characterised by crest displacements of 3 cm or less, corresponding to accelerations of 0.3 g or less, as indicated in Figure 21. However, at higher demands, the continuous

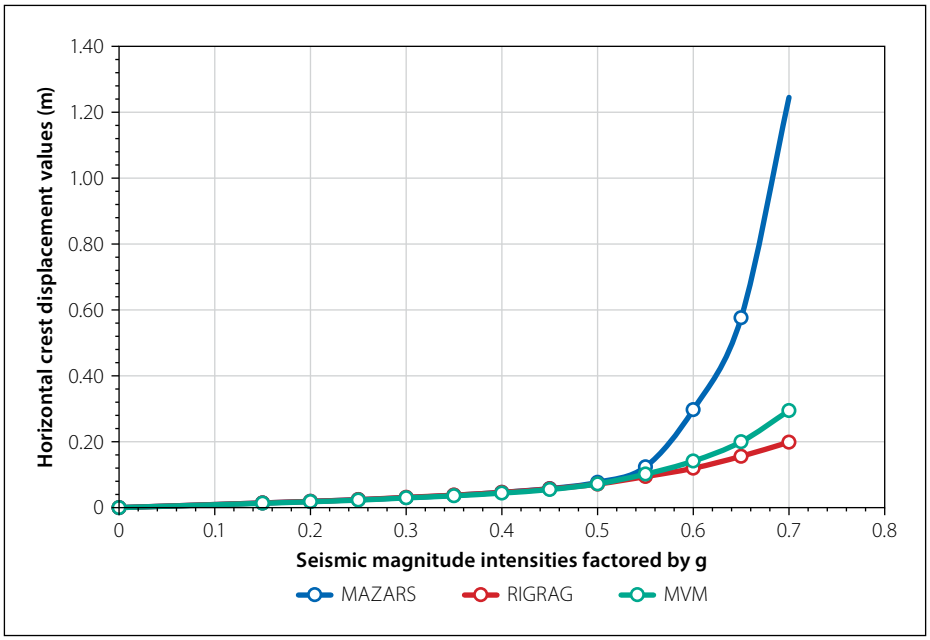

Figure 21 Horizontal crest displacement obtained by the three damage models

mesh models demonstrate a significant increase in capacity. Notably, the RICRAG model exhibits a 62% superiority at a demand of 13 cm. Similarly, the Mazars and MVM models display superiorities of 52% and 54.7% at demands of 10 cm and 14 cm, respectively. These observations suggest that the seismic capacities of continuous mesh models might be overestimated for moderate and strong earthquakes. Conversely, interface models demonstrate a greater displacement capacity. Additionally, among the three damage models, the Mazars model demonstrates a larger deformation before divergence, implying greater ease of use in numerical simulations.

CONCLUSION

In conclusion, this study highlights the enhanced precision of calculation models for gravity dams when considering the interface between the dam and the foundation. This was not only confirmed when utilising damage models, but also when incorporating a step abutment at the interface. The necessity for employing this model becomes more apparent when simulating earthquakes of significant magnitudes surpassing accelerations of approximately 0.35 g.

However, difficulties associated with stress concentration phenomena may arise due to zones with steep deformation gradients, resulting from sharp and non-rounded angles in the geometric shape of these abutments. To provide more accurate recommendations regarding the treatment of these zones during construction, further numerical investigations into the attenuation effects of these stress concentration phenomena within both the dam and the foundation need to be undertaken.

REFERENCES

Bažant, Z P 1986. Mechanics of distributed cracking. *Applied Mechanics Reviews*, 39(5): 675–705.

Bažant, Z P & Pijaudier-Cabot, G 1989. Measurement of characteristic length of non-local continuum. *Journal of Engineering Mechanics*, 115(4): 755–767.

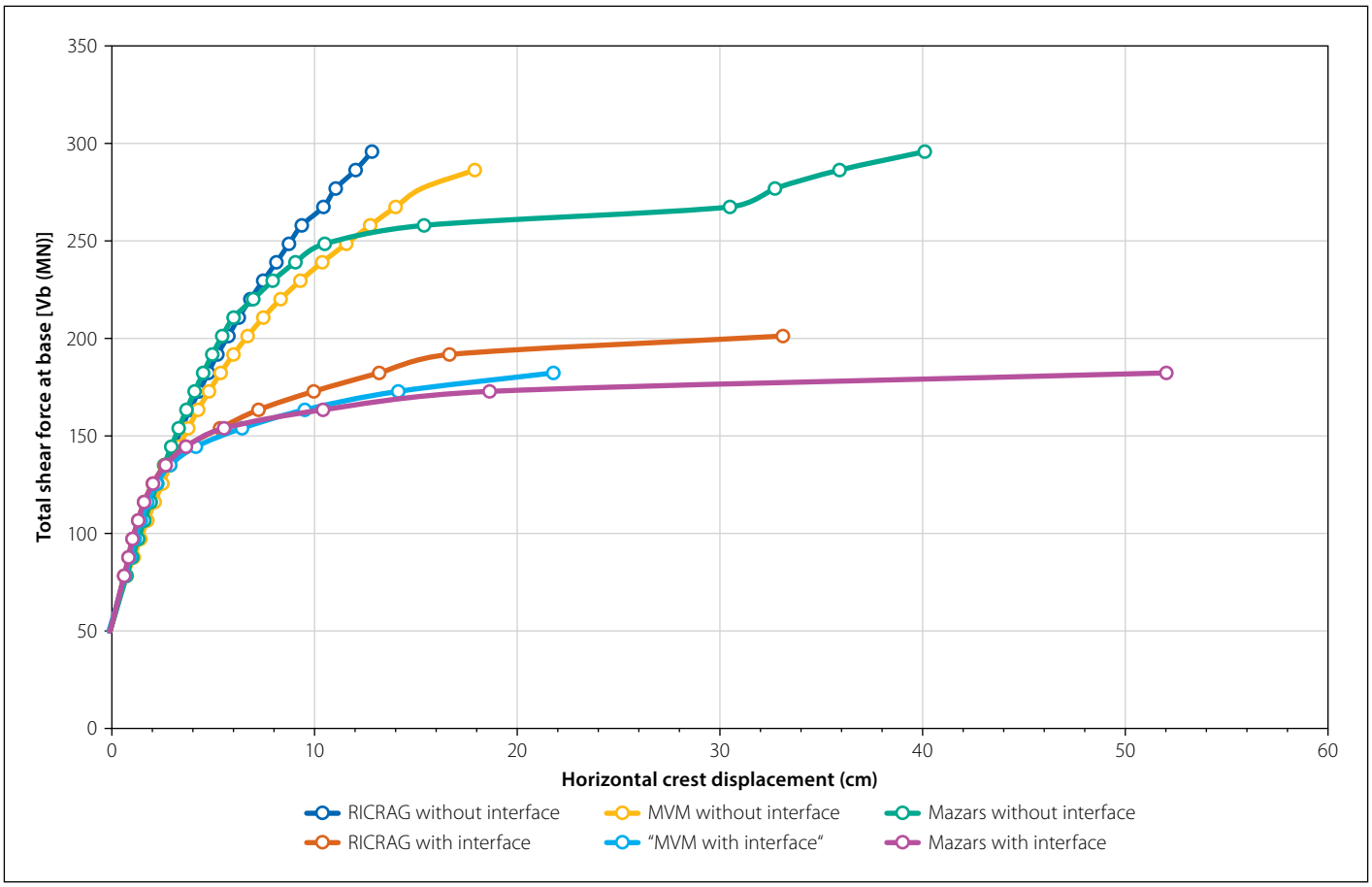

Figure 22 Seismic capacity curves for continuous and discontinuous mesh damage models

Becheur, A, Medjahed, A & Coorevits, P 2018. A new *a posteriori* error indicator and its mesh optimization for non-local concrete damage models. *Latin American Journal of Solids and Structures,* 15: e104. DOI: 10.1590/1679-78254793.

Bhattacharjee, S S & Léger, P 1994. Application of NLFM models to predict cracking in concrete gravity dams. *Journal of Structural Engineering,* 120(4): 1255–1271.

Cai, Q, Robberts, J M & Van Rensburg, B W J 2008. Finite element fracture modelling of concrete gravity dams. *Journal of the South African Institution of Civil Engineering,* 50(1): 13–24.

Calayir, Y & Karaton, M 2005. A continuum damage concrete model for earthquake analysis of concrete gravity dam–reservoir systems. *Soil Dynamics and Earthquake Engineering*, 25(11): 857–869.

Cast3M 2023 *Finite Element Analysis (FEA) code.* Available at: http://www-cast3m.cea.fr/ (accessed on 20 May 2024).

De Vree, J H P, Brekelmans, W A M & Van Gils, M 1995. Comparison of non-local approaches in continuum damage mechanics. *Computers & Structure,* 55(4): 581–588.

Durieux, J H & Van Rensburg, B W J 2016. Development of a practical methodology for the analysis of gravity dams using the non-linear finite element method. *Journal of the South African Institution of Civil Engineering*, 58(2): 2–13. DOI: 10.17159/2309-8775/2016/v58n2a1.

Enzell, J, Malm, R, Abbasiverki, R & Ahmed, L 2021. Non-linear behaviour of a concrete gravity dam during seismic excitation: A case study of the Pine Flat Dam. In: Bolzon, G, Sterpi, D, Mazzà, G & Frigerio, A (Eds). *Numerical Analysis of Dams* (Lecture Notes in Civil Engineering). Cham, Switzerland: Springer International Publishing, 99–112. DOI: 0.1007/978-3-030-51085-5_2.

Faggiani, G, Masarati, P & Frigerio, A 2021. Assessment of the dynamic response of pine flat concrete gravity dam. FEM simulation of dam-foundation interaction. In: Bolzon, G, Sterpi, D, Mazzà, G & Frigerio A (Eds). *Numerical Analysis of Dams* (Lecture Notes in Civil Engineering). Cham, Switzerland: Springer International Publishing, 113–127. DOI: 10.1007/978-3-030-51085-5_3.

Giry, C, Dufour, F & Mazars, J 2011. Stress-based non-local damage model. *International Journal of Solids and Structures,* 48(25–26): 3431–3443.

Jabbar, A A, Irzooki, R H & Al-Obaidi, A A 2021. Improving resistance of gravity dam to seismic wave by using stepped base. In: *E3S Web of Conferences,* Vol 318. Available at: https://www.e3s-conferences.org.

Kachanov, L M 1958. On creep rupture time. *Izvestiya Akademii Nauk SSSR, Otdelenie Tekhnicheskikh Nauk,* 8: 26–31.

Lee, J & Fenves, G L 1998. A plastic-damage concrete model for earthquake analysis of dams. *Earthquake Engineering & Structural Dynamics*, 27(9): 937–956. DOI: 0.1002/(SICI)1096-9845(199809)27:9<937:AID-EQE764>3.0.CO;2-5.

Léger, P & Leclerc, M 1996. Evaluation of earthquake ground motions to predict cracking response of gravity dams. *Engineering Structures,* 18(3): 227–239.

Mazars, J 1986. A description of micro- and macroscale damage of concrete structures. *Engineering Fracture Mechanics*, 25(5):729–737. DOI: 10.1016/0013-7944(86)90036-6.

Needleman, A 1988. Material rate dependence and mesh sensitivity in localization problems. *Computer Methods in Applied Mechanics and Engineering,* 67(1): 69–85.

Pegon, P & Anthoine, A 1997. Numerical strategies for solving continuum damage problems with softening: Application to the homogenization of masonry. *Computers & Structures,* 64(1): 623–642. DOI: 10.1016/S0045-7949(96)00153-8.

Pijaudier-Cabot, G & Bažant, Z P 1987. Non-local damage theory. *Journal of Engineering Mechanics,* 113(10): 1512–1533.

Pijaudier-Cabot, G, Mazars, J & Pulikowski, J 1991. Steel-concrete bond analysis with non-local continuous damage. *Journal of Structural Engineering,* 117(3): 862–882. DOI: 10.1061/(ASCE)0733-9445(1991)117:3(862).

Rabotnov, Y N 1959. On the mechanism of the long-term fracture. In: *Problems in the Strength of Materials and Structures.* Moscow: USSR Academy of Sciences, 5–7.

Richard, B, Ragueneau, F, Cremona, C & Adelaide, L 2010. Isotropic continuum damage mechanics for concrete under cyclic loading: Stiffness recovery, inelastic strains and frictional sliding. *Engineering Fracture Mechanics,* 77(8): 1203–1223.

Si-Chaib, A, Tardieu, B, Abidi, M-K, Molin, X & Lignier, P 2018. Prediction of gravity dams' behaviour under strong earthquakes. (Part II): Application to Beni-Haroun Dam. In: Fry, J-J & Matsumoto, N (Eds). *Validation of Dynamic Analyses of Dams and Their Equipment.* London: CRC Press, 593–608.

Vorlet, S, Manso, P & De Cesare, G 2021. Seismic behaviour of Pine Flat concrete gravity dam using microplane damage-plasticity model. In: Bolzon, G., Sterpi, D., Mazzà, G & Frigerio, A (Eds.) *Numerical Analysis of Dams* (Lecture Notes in Civil Engineering). Cham, Switzerland: Springer International Publishing, 353–367. doi.org/10.1007/978-3-030-51085-5_19.

Westergaard, H M 1933. Water pressures on dams during earthquakes. *Transactions of the American Society of Civil Engineers,* 98(2): 418–433. DOI: 10.1061/TACEAT.0004496.

Zreid, I & Kaliske, M 2018. A gradient enhanced plasticity–damage microplane model for concrete. *Computational Mechanics,* 62(5):1239–1257. DOI: 10.1007/s00466-018-1561-1.